IEEE Access
Multidisciplinary ⋮ Rapid Review ⋮ Open Access Journal

Received 12 January 2023, accepted 14 February 2023, date of publication 24 February 2023, date of current version 7 March 2023.

Digital Object Identifier 10.1109/ACCESS.2023.3246093

RESEARCH ARTICLE

Ship Formation Algorithm Based on the Leader–Follower Method

MINGYANG LI[1], KAI MENG[1], JIELU CHEN[2], AND HONGBO WANG[1], (Member, IEEE)
[1]State Key Laboratory on Integrated Optoelectronics, College of Electronic Science and Engineering, Jilin University, Changchun 130012, China
[2]CSSC Marine Technology Company Ltd., Pudong, Shanghai 200136, China

Corresponding author: Hongbo Wang (wang_hongbo@jlu.edu.cn)

This work was supported in part by the National Natural Science Foundation of China (NSFC) under Grant u1964202.

ABSTRACT In recent years, marine engineers have increasingly relied on multiship collaborative work to complete complex tasks at sea and improve maritime transport efficiency. Ship formation significantly contributes to the maintenance of stability during multiship-coordinated operations, but establishing the formation structure while ensuring the safety of each ship remains challenging. Therefore, this study proposes an improved leader–follower-based formation algorithm as a solution to this issue. First, the fast marching square method was used for global static path planning. The leader–follower formation control method then enabled the path tracking of the follower ship to the leader ship. Finally, an improved artificial potential field method was used for local collision avoidance, and virtual obstacles were added to improve the situation in which the ship probably entered a local minimum point. The experimental results revealed that the proposed algorithm could plan a route with time, smoothness, and safety advantages for the formation leader and quickly form a stable formation. Notably, the ship can quickly initiate collision avoidance operations when it encounters an obstacle posing a collision risk.

INDEX TERMS Artificial potential field method, fast marching square method, formation of ships, leader–follower method, local collision, path planning.

I. INTRODUCTION

Most traditional ship motion research objects are single ships, but single ships frequently have significant operational limitations. Owing to the complexity and diversification of navigation and marine operation tasks in recent years, multiple sea surface ships must collaborate to accomplish complex tasks that a single ship cannot, such as fleet cooperative operation, search and rescue, fleet roundup, and marine resource exploration. With the rapid advancement and integration of communication and computer technology, the problem of the cooperative formation of surface ships has received increased attention from scholars around the globe. Notably, the study of ship formation systems is of great theoretical value and practical engineering significance because such systems have greater fault tolerance, adaptability, and working efficiency than traditional single ships when confronting complex tasks [1], [2].

Ship navigation relies heavily on path planning, which can be divided into global and local. Based on task requirements, global path planning uses advanced data such as electronic charts and appropriate search algorithms to find a feasible, barrier-free route in a large area [3], [4], [5], [6]. Local path-planning algorithms play an auxiliary role in global navigation systems. During global path navigation, the ship detects and autonomously avoids unknown obstacles. After completing the avoidance, the ship returns to its global path [7], [8], [9], [10].

Currently, the most commonly used global path-planning algorithms include Dijkstra [11], [12], [13], A* [14], [15], genetic [16], [17], [18], particle swarm optimization [19], [20], [21], and ant colony algorithms [22]. Dijkstra and A* algorithms are used to solve the optimal path. The Dijkstra algorithm was first proposed by Dijkstra [23] in 1959. The classic Dijkstra algorithm has a simple underlying principle,

The associate editor coordinating the review of this manuscript and approving it for publication was Emre Koyuncu.

but its calculation process is overly complex and memory-intensive, making it unsuitable for large-scale path planning. Moreover, the A* algorithm is a heuristic algorithm proposed by Hart et al. [24]; this algorithm is the most effective method for determining the shortest path in static networks, extending Dijkstra's algorithm. Although the A* algorithm has a simple underlying principle and outperforms the Dijkstra algorithm, it relies heavily on the heuristic function, resulting in a massive amount of computation, and both algorithms require additional smoothing. Furthermore, James proposed a numerical method called fast marching to solve the Eikonal equation's boundary value problem [25]. This method generates potential fields by simulating the propagation of electromagnetic waves as they travel from their source point to their destination. The potential field simulated by this method has only one global minimum point, the starting point, and its path is generated by the gradient descent method, which effectively avoids the problem of a local minimum. Based on this, the enhanced fast marching square method is suitable for ship tracking due to its excellent smoothness and security.

The current local path planning algorithms mainly include fuzzy logic algorithm [26], [27], artificial potential field method [28], [29], [30], [31], velocity obstacle method [32], [33] and so on. Guan et al. proposed a ship domain model based on fuzzy logic aimed at providing early warning of ship collision risk and a reasonable reference that can be used in combination with the International Regulation for Preventing Collisions at Sea [26]. Shang et al. designed a fuzzy controller to improve the problem of trajectory oscillation, which outputs the environment danger factor to adjust the step size of robot and enhance the trajectory smoothness of robot in complex environment [27]. Yang studied the development process of the obstacle avoidance system for autonomous vehicles and propose an optimization scheme for the obstacle avoidance algorithm [28]. Chen and Xu proposed a method of removing the shaking state based on a favorable path, and on this basis, visibility graph method is used to optimize the path of the AUV to avoid obstacles [31]. Wang et al. proposed a USV autonomous dynamic obstacle avoidance method based on the enhanced velocity obstacle method in order to achieve path replanning [32].

However, in local path planning algorithms, ships often work in a partially or completely unknown environment, which requires continuous detection of the surrounding environment by sensors. According to the data detected by the sensors: the distance, size, shape, etc. between the obstacle and the ship itself, its position, speed, and direction are constantly adjusted. This obstacle avoidance method requires the performance of the ship's own sensors to be very powerful, and the designed algorithm should be more and more accurate and practical. The artificial potential field method is a more mature and effective algorithm, which allows moving objects to avoid obstacles while considering the motion performance of moving objects. It has the advantages of strong real-time performance, simple mathematical calculation, smooth path planning, and easy programming. Therefore, this paper uses the artificial potential field method to realize the local path planning of the ship.

With the maturation of the single ship control theory, Professor Fossen and his team initiated research into multiship cooperative formation control in 2002 [34]. Many important theoretical and technical advances have been made in the study of formation control of surface ships, thanks to the collaboration of international navigation and control circles. Because maintaining formation stability is crucial for ship formation, inspired by the behaviors of birds gathering, ant colonies, and bee swarms, researchers have proposed various formation structures, such as leader–follower, virtual structure [35], [36], [37], [38], [39], and behavior-based methods [40], [41], [42].

Among these formation methods, the formation control method based on leader-follower method has the advantages of simple principle and easy implementation, which is favored by scholars. The leader–follower method adopts a centralized control structure. The basic concept is to designate one or more team members as leaders and the rest as followers. The leader can track the desired trajectory and posture, and the follower can communicate with the leader. Meanwhile, maintaining relative distance, azimuth, and attitude consistency with the pilot is essential for achieving formation control of a particular formation. Ding and Guo [43] studied the surface ship formation problem based on the leader-follower method. By designating one ship in a multiship system as the system's leader and the other ships as its followers, the formation problem was viewed as the following and coordination problem of all following ships to the position and direction of the system's leader. Liu et al. used control theory to investigate the controllability of a leader–follower multiagent system in switched communication topology and presented the system's controllability conditions in this setting [44]. Ajwad et al. studied the same system based on a continuo–discrete observer and demonstrated the proposed algorithm's stability using Lyapunov theory [45]. Wang et al. also studied the consistency of the aforementioned system under a directed hostile communication topology [46].

This paper proposes an improved leader-follower formation algorithm to establish the formation structure and ensure the safety of the formation. The global static path planning is carried out by the fast marching square method, and it is combined with the leader-following method for the first time to realize the path tracking from the follower ship to the leader ship. Notably, the preceding studies did not consider the possible obstacles encountered by followers during navigation. Therefore, this study proposes an improved artificial potential field method to solve this problem, enabling the follower to independently take collision avoidance behavior when collision risk occurs during the trajectory tracking of the leader and to return to the team after a collision avoidance operation.

The remainder of this paper is structured as follows. Section II introduces the basic concepts and applications of

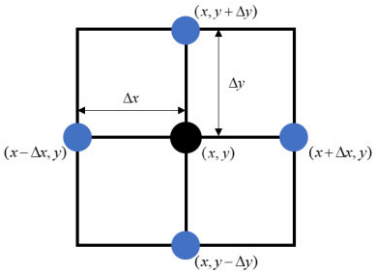

FIGURE 1. 2D discrete space.

the fast marching and fast marching square methods, revealing how the latter plans a collision-free path for the ship's leader. Section III presents the basic knowledge of graph theory and its application to ship formation. The consistency theory is adopted to solve the tracking problem of the follower to the leader and realize the effect of formation keeping. Section IV presents an improved artificial potential field method for solving the local collision avoidance problem, enabling followers to take collision avoidance behavior independently. Section V presents the simulation and analysis of the proposed algorithm. Finally, Section VI concludes the study.

II. FAST MARCHING METHOD AND FAST MARCHING SQUARE METHOD

A. FAST MARCHING METHOD

1) PROPOSAL OF THE FAST MARCHING METHOD

In 1996, J. Sethian first proposed a numerical algorithm, the fast marching method (FMM), which can approximate the viscosity solution of an equation, and used this algorithm to iteratively solve the Eikonal equation to solve the interface propagation problem.

The function equation has the following form:

$$|\nabla T(x, y)|\, W(x, y) = 1, \tag{1}$$

where (x, y) is the coordinates in the position and pose space of the calculated point, $T(x, y)$ is the time when the interface reaches the point (x, y), and $W(x, y)$ is the local propagation speed of the interface at the point (x, y).

Although the FMM used to solve the Eikonal equation shares commonalities with the Dijkstra method, the Dijkstra algorithm updates based on Euclidean distance between nodes, whereas the FMM algorithm updates based on the approximate partial differential equation obtained from the simplified Eikonal equation.

To use FMM, the space must be discretized. Fig. 1 shows a discrete 2D space. The Eikonal equation can be written as follows:

$$\max(\frac{T - T_x}{\Delta x}, 0)^2 + \max(\frac{T - T_y}{\Delta y}, 0)^2 = \frac{1}{F_{ij}^2}, \tag{2}$$

where $T_x = \min(T_{(x-\Delta x,y)}, T_{(x+\Delta x,y)})$, $T_y = \min(T_{(x,y-\Delta y)}, T_{(x,y+\Delta y)})$.

Notably, the solution set for time T in this equation can be obtained as follows:

Case 1: When $T > \max(T_x, T_y)$, the Eikonal equation can be written as

$$(\frac{T - T_x}{\Delta x})^2 + (\frac{T - T_y}{\Delta y})^2 = \frac{1}{F_{ij}^2}. \tag{3}$$

Assuming that the unit distance between the horizontal and vertical discrete points is 1, i.e., $\Delta x = \Delta y = 1$, then the Eikonal equation can be reduced to a quadratic equation of one variable:

$$(T - T_x)^2 + (T - T_y)^2 = \frac{1}{F_{ij}^2}, \tag{4}$$

$$T^2 - (T_y + T_x)T + \frac{1}{2}(T_y^2 + T_x^2 - \frac{1}{F_{ij}^2}) = 0. \tag{5}$$

Thus, the solution of time T can be written as follows:

$$T = \frac{T_x + T_y + \sqrt{\frac{2}{F_{ij}^2} - (T_x - T_y)^2}}{2}. \tag{6}$$

Because the other solution of time T is negative, it does not satisfy the condition and is thus dropped.

Now, determine whether the solution satisfies the assumptions, i.e., if the following inequality is true:

$$T = \frac{T_x + T_y + \sqrt{\frac{2}{F_{ij}^2} - (T_x - T_y)^2}}{2} > \max(T_x, T_y). \tag{7}$$

Let $T_x \geq T_y$, that is

$$T = \frac{T_x + T_y + \sqrt{\frac{2}{F_{ij}^2} - (T_x - T_y)^2}}{2} > T_x. \tag{8}$$

The solution to this inequality is

$$T = T_2 + \frac{1}{F_{ij}}. \tag{9}$$

Case 2: when $T_1 \geq T > T_2$, the Eikonal equation can be written as follows:

$$(T - T_2)^2 = \frac{1}{F_{ij}^2}, \tag{10}$$

where $T_1 = \max(T_x, T_y)$, $T_2 = \min(T_x, T_y)$.

The solution to this equation is

$$T = T_2 + \frac{1}{F_{ij}}. \tag{11}$$

Because the other solution of time T is negative, it does not satisfy the condition and is thus dropped.

Now, determine whether the solution satisfies the assumptions, i.e., if the following inequality is true:

$$T = T_2 + \frac{1}{F_{ij}} \leq T_1. \tag{12}$$

The solution to this inequality is

$$T_1 - T_2 \geq \frac{1}{F_{ij}}, \tag{13}$$

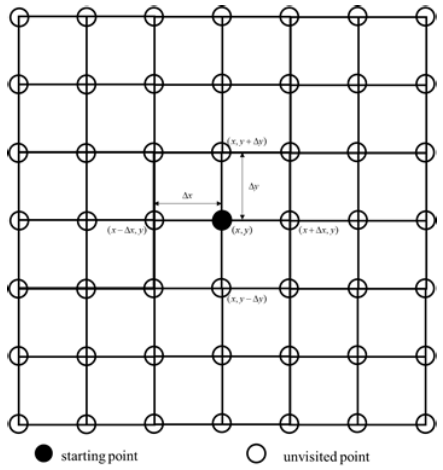

FIGURE 2. Initializing the map.

which is

$$|T_x - T_y| \geq \frac{1}{F_{ij}}. \tag{14}$$

Overall, the solution set of T can be written as follows:

$$T = \begin{cases} \dfrac{T_x + T_y + \sqrt{\dfrac{2}{F_{ij}^2} - (T_x - T_y)^2}}{2}, & |T_x - T_y| < \dfrac{1}{F_{ij}} \\ \min(T_x, T_y) + \dfrac{1}{F_{ij}}, & |T_x - T_y| \geq \dfrac{1}{F_{ij}}. \end{cases} \tag{15}$$

2) DESCRIPTION OF THE FAST MARCHING METHOD ALGORITHM

The algorithm description of FMM is shown in Algorithm 1.

- Step 1: The navigation environment is modeled and converted into a binary grid diagram. Separate the cells that belong to the barrier and the cells that correspond to the passable area.
- Step 2: FMM divides points on the map into three groups: frozen, open, and unvisited points. Frozen points are points at which the arrival time can no longer be changed. Unvisited points are unprocessed points. Open points can be thought of as the interface between the frozen and unvisited areas of the map belonging to the propagation surface. In the path-planning problem, to ensure that only one global minimum point exists, the wave propagates from the target point. As shown in Fig. 2, in this step, all cells in the point set are initialized to an infinite value and set to unvisited points, except that the propagation starting point is set to an arrival time of 0.
- Step 3: In each iteration, the open point comprises four adjacent grids of a black sphere (marked blue), as shown in Fig. 3. The open point with the smallest T-value is then selected as the frozen point by solving the formula. As shown in Fig. 4, the process continues until the end condition of interface propagation theoretically covers all feasible areas for the iteration result or until all points are set to frozen points or reach the starting point of the path-planning problem.

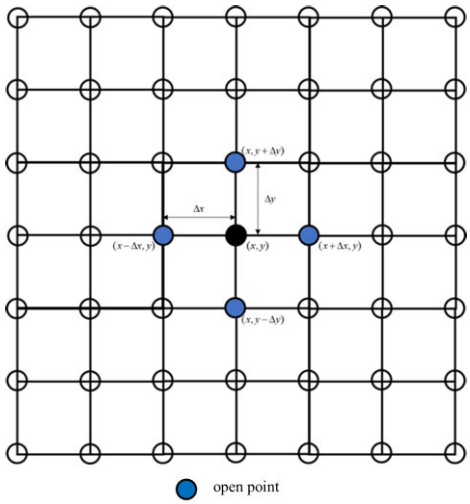

FIGURE 3. The first iteration.

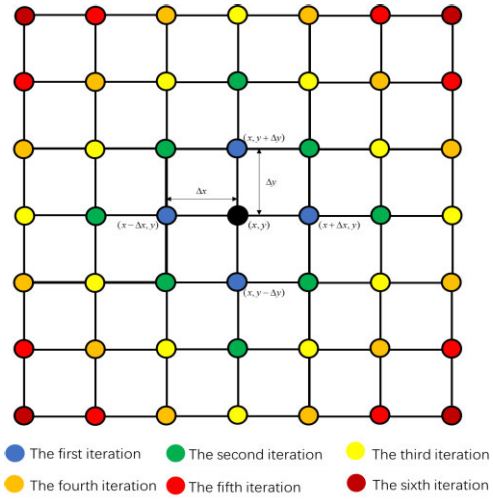

FIGURE 4. Iterative process.

Each grid point's value in this constructed potential field represents the arrival time of the interface. Notably, the interface cannot propagate in the infeasible region; that is, the propagation speed of the interface in the infeasible region is 0, and the arrival time approaches infinity. If the interface travels at the same speed throughout the map, the arrival time of the interface is proportional to the distance from the starting point of the current grid data.

B. FAST MARCHING SQUARE METHOD

The essence of FMM is to search for the interface's shortest propagation path. The path length is prioritized over path safety and smoothness. If you drive along the path generated by the FMM, only the shortest distance is guaranteed, and safety cannot be ensured.

This study uses the fast marching square (FMS) method to calculate a path with sufficient smoothness and safe distance,

Algorithm 1 Fast Marching Method Algorithm Description

Input: The velocity of a point in a 2-dimensional discrete space F_{ij},
Point set S, Discrete space step size Δh,
Output: Time T

$\forall p \notin S, T(p) = +\infty$
for $p \in S$ **do**
  $ps = Neighbor(p)$
  $T(ps) = T(p) + \Delta h$
  $Trial \leftarrow ps, Alive \leftarrow S$
end for
while $Trial \neq \emptyset$ **do**
  $m = \min(Trial)$
  $Alive \leftarrow m$
  $ms = Neighbor(m)$
  for $\forall p \in S, p \notin Alive$ **do**
  $\{i, j\} = p$
  $T_x = \min(T_{(i-\Delta h,j)}, T_{(i+\Delta h,j)})$
  $T_y = \min(T_{(i,j-\Delta h)}, T_{(i,j+\Delta h)})$
  if $\left|T_x - T_y\right| < \frac{\Delta h}{F_{ij}}$ **then**
  $T = \frac{T_x + T_y + \sqrt{\frac{2}{F_{ij}^2} - (T_x - T_y)^2}}{2} > T_x$
  else
  $T = \min(T_x, T_y) + \frac{1}{F_{ij}}$
  end if
  $T(p) = \min\{T(p), T\}$
  $Trail \leftarrow p$
  end for
return T

addressing the path defects generated directly by FMM, notably that the path is too close to the obstacle and is not smooth.

FMS applies the basic FMM twice.

- Step 1: The environment is modeled similarly to when FMM is used. Convert the environment into a binary grid. Separate the cells that belong to the barrier and the cells that correspond to the passable area.
- Step 2: By applying FMM for the first time, FMS treats each obstacle-marked cell on the map as a wave source and simultaneously expands multiple waves. The resultant value of each map cell represents the time required for the wave to reach the nearest obstacle, which is proportional to the obstacle's distance. The potential diagram obtained from this step is the velocity potential $W(x)$.
- Step 3: Based on the potential diagram $W(x)$, FMM is executed again from the target point. This time, the target point is treated as the only wave source to ensure a global minimum. The wave expands across the map until it reaches its initial point. For each cell in the feasible region, the wave expansion velocity is extracted from the velocity potential diagram $W(x)$ calculated in the previous step.
- Step 4: From the ship's starting point, a gradient descent is made across the entire arrival time map, moving toward its target point (the global minimum of the resulting map). By using FMS, a path that incorporates arrival time, smoothness, and safety is obtained.

In this section, FMS solves the global path-planning problem and provides the formation leader with the planned path to track. Then, the subsequent section will solve the problem of how to realize the tracking of the follower to the leader in order to maintain formation stability.

III. LEADER–FOLLOWER SHIP FORMATION

A. STRUCTURE OF THE SHIP FORMATION

With the development of ship clustering technology, which was inspired by natural behaviors, such as bird gathering, ant colonies, and bee swarms, researchers began exploring ways to control multiple smart ships simultaneously, resulting in the creation of ship formation technology. The implementation of ship formation technology can increase efficiency and performance while addressing the shortcomings of single ships, such as inadequate carrying capacity and insufficient information processing capacity. Simultaneously, the stability and safety of ship formation are improving thanks to advancements in computer science and technology, communication technology, and navigation technology.

Typical cluster collaborative control technologies include leader–follower, virtual structure, and behavior-based methods.

The virtual structure approach treats the entire system as a rigid-body structure, with the individuals making up the formation serving as the rigid body's reference points with fixed relative positions. When the entire body is in motion, each individual can achieve a fixed shape formation motion by tracking the corresponding reference points on the rigid body. Group behavior can be easily programmed using this method, which also yields excellent results in the areas of trajectory tracking and formation keeping.

The fundamental concept underlying the behavioral method is as follows: first, the agent's expected basic behaviors are specified. In general, behaviors include collision avoidance, obstacle avoidance, target-directed driving, and formation maintenance. When the sensor is stimulated by the external environment, it responds based on the sensor's input information and outputs the response vector as the expected behavior response.

The benefits of the leader–follower method include a simple principle, easy implementation, and good stability. As a result, this study uses a centralized control structure in which one ship acts as the formation leader and the others act as its followers.

As a global path-planning algorithm, FMS described in Section II can be used to plot the course of a ship formation's leader. In this section, we will determine how to maintain the relative distance and azimuth between the follower and leader.

B. FOUNDATION OF GRAPH THEORY

In general, multiagent formation control has a large scale, and each individual has a communication and control relationship that can form a network structure. Therefore, the multiagent system can be modeled naturally as a graph. The graph vertex typically represents a single agent. The graph edges represent the topological relationships between agents.

After the multiagent system is modeled as a graph, the formation problem can be studied using the relevant knowledge of graph theory. Graph theory methods make it simple to design team shapes and formation control algorithms.

1) LAPLACIAN MATRIX

The Laplacian matrix, also known as the admittance matrix, Kirchhoff matrix, or discrete Laplacian operator, is mainly used in graph theory. As a matrix representation of a graph, the Laplacian matrix can reflect the degree of graph connectivity while describing the point–edge relationship in the graph.

Given a figure $G = \{V, E\}$, as shown in Fig. 5, $V = \{v_1, v_2, \ldots, v_n\}$ represents the vertices in the graph, $E \subset v \times v$ is the graph edge; the Laplacian matrix is defined as $L = D - A$, where D stands for the degree matrix and A is the adjacency matrix.

The degree matrix is a diagonal matrix whose diagonal value is the sum of the total number of adjacent nodes that maintain a communication relationship with each vertex in the graph. The degree matrix in this graph is

$$D = \begin{pmatrix} 2 & & & & & \\ & 2 & & & & \\ & & 3 & & & \\ & & & 3 & & \\ & & & & 2 & \\ & & & & & 2 \end{pmatrix}. \tag{16}$$

The adjacency matrix is a symmetric matrix whose value on the main diagonal is 0. If a communication relationship exists between points v_i and v_j, then $a_{ij} = a_{ji} = 1$; otherwise, $a_{ij} = a_{ji} = 0$. The adjacency matrix is

$$A = \begin{pmatrix} 0 & 1 & 1 & 0 & 0 & 0 \\ 1 & 0 & 1 & 0 & 0 & 0 \\ 1 & 1 & 0 & 1 & 0 & 0 \\ 0 & 0 & 1 & 0 & 1 & 1 \\ 0 & 0 & 0 & 1 & 0 & 1 \\ 0 & 0 & 0 & 1 & 1 & 0 \end{pmatrix}. \tag{17}$$

Thus, the Laplacian matrix can be written as

$$L = D - A = \begin{pmatrix} 2 & -1 & -1 & 0 & 0 & 0 \\ -1 & 2 & 1 & 0 & 0 & 0 \\ -1 & -1 & 3 & -1 & 0 & 0 \\ 0 & 0 & -1 & 3 & -1 & -1 \\ 0 & 0 & 0 & -1 & 2 & -1 \\ 0 & 0 & 0 & -1 & -1 & 2 \end{pmatrix}. \tag{18}$$

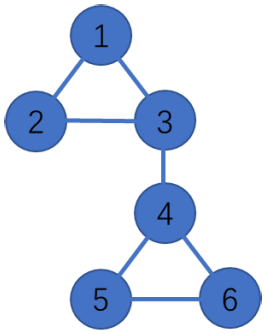

FIGURE 5. Undirected connected graphs.

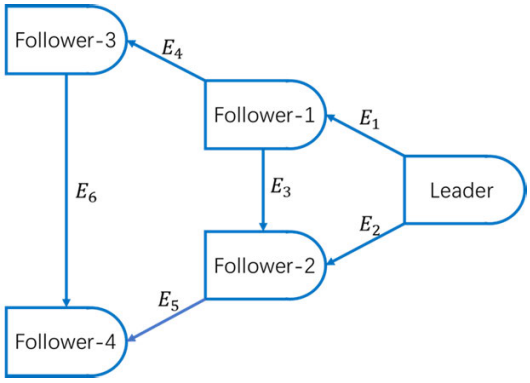

FIGURE 6. Leader–follower multiship formation system.

2) APPLICATION OF THE LAPLACIAN MATRIX IN SHIP FORMATION

The leader–follower multiship formation system treats each ship in the system as a network node and the information transmission link between ships as an edge connecting different nodes. Thus, a multiship system and its communication network can be modeled as a diagram. However, unlike the undirected graph introduced in Section III, Part B(1), due to the existence of information flow in formation, the ship formation system is constructed as a directed graph, as shown in Fig. 6, where the arrow direction represents the direction of information transmission.

Given the directed graph $G = \{V, E\}$, $V = \{v_1, v_2, \ldots, v_n\}$ represents the vertices in the graph, i.e., N ships in the system, $E \subset v \times v$ is the graph edge.

In this digraph, the adjacency matrix A is transformed into a weight matrix; if vertex v is the starting point of edge E, then $a_{ij} = 1$, otherwise $a_{ij} = 0$. The degree matrix D is transformed into an indegree matrix, with the diagonal elements representing the sum of the nodes' intake degree.

Thus, the weight matrix of the system can be written as follows:

$$A = \begin{pmatrix} 0 & 0 & 0 & 0 & 0 \\ 1 & 0 & 0 & 0 & 0 \\ 1 & 1 & 0 & 0 & 0 \\ 0 & 1 & 0 & 0 & 0 \\ 0 & 0 & 1 & 1 & 0 \end{pmatrix}. \tag{19}$$

The indegree matrix is as follows:

$$D = \begin{pmatrix} 0 & & & & \\ & 1 & & & \\ & & 2 & & \\ & & & 1 & \\ & & & & 2 \end{pmatrix}. \tag{20}$$

The Laplacian matrix can be written as follows:

$$L = D - A = \begin{pmatrix} 0 & 0 & 0 & 0 & 0 \\ -1 & 1 & 0 & 0 & 0 \\ -1 & -1 & 2 & 0 & 0 \\ 0 & -1 & 0 & 1 & 0 \\ 0 & 0 & -1 & -1 & 2 \end{pmatrix}. \tag{21}$$

Define $x = [x_1, x_2, \ldots x_5]^T$ as the current coordinate value of each ship and η as the expected relative positions of adjacent two points.

Thus, for each edge on the digraph, we can obtain the following:

The error of the expected distance from point x_j to point x_i is as follows:

$$e_{ij} = x_i - x_j - \eta. \tag{22}$$

The sum of the errors of the expected distance between point x_j and all other points is as follows:

$$e_j = \sum_i e_{ij} = Ax - Dx - k\eta = -Lx - k\eta. \tag{23}$$

To enable the follower to track the leader's trajectory, we must reduce the value of e_j to 0, thereby affecting the speed of each follower by e_j and achieving formation stability by eliminating the error.

IV. LOCAL COLLISION AVOIDANCE BASED ON AN IMPROVED ARTIFICIAL POTENTIAL FIELD METHOD

In Section III, we used the leader–follower method to track the leader's path, allowing the ship team to reach the end point stably. The analysis in the preceding section reveals, however, that the follower in the team follows only the leader mechanically. When the follower is too close to an obstacle on the tracked path, the collision risk is likely to materialize. Therefore, each follower must independently achieve local collision avoidance in order to deal with this situation. This section focuses on the independent collision avoidance of each follower when encountering collision risk, as well as on the maintenance of collision avoidance within the formation.

The artificial potential field method proposed by KHATIB [47] establishes a constraint relationship among ships, target positions, and obstacles through a virtual force field. When sailing in formation, the follower ship naturally receives the gravitational force brought about by the preset target position of the formation. However, if it senses that the distance to the obstacle is too close, it will enter collision avoidance mode and experience extra repulsive force from the obstacle. The follower ship will move under the combined influence of gravity and repulsive force until it can avoid the obstacle and reach a safe area.

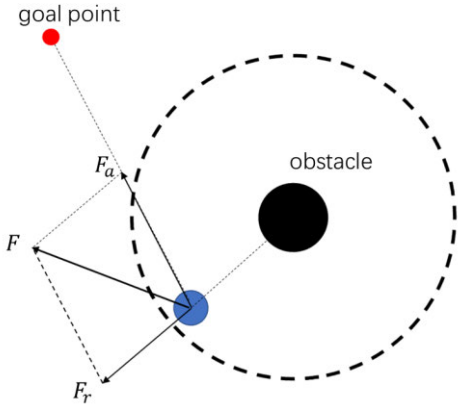

FIGURE 7. Schematic diagram of the artificial potential field method.

A. ARTIFICIAL POTENTIAL FIELD

Fig. 7 is a schematic representation of the artificial potential field method.

Assuming that the real-time coordinate position of the ship is $X = (x, y)$ and the position of the target point is $X_g = (x_g, y_g)$, then the gravitational field function is

$$U_a = \frac{1}{2}k(X - X_g)^2, \tag{24}$$

where the coefficient k is the gain coefficient of the gravitational field, and the appropriate constant is selected by the experiment.

Notably, the size of the gravitational field is positively correlated with the distance between the ship and the target point.

The following relation can be derived from the relationship between gravitation and gravitational field:

$$F_a = -grad(U_a) = -k(X - X_g). \tag{25}$$

In the artificial potential field method, the repulsive force is inversely proportional to the square of the distance of the obstacle. That is, as the distance to the obstacle decreases, the repulsion intensifies and vice versa. However, the influence of obstacles on ships is not infinite and only has an effect within a certain range, as indicated by the black dotted line area in Fig. 7. The repulsive force becomes 0 outside this range. The mathematical expression of the repulsive force field is

$$U_r = \begin{cases} \frac{1}{2}\beta(\frac{1}{\rho} - \frac{1}{\rho_0})^2 & \rho \le \rho_0 \\ 0 & \rho > \rho_0, \end{cases} \tag{26}$$

where the coefficient β is the gain coefficient of the repulsive force field, ρ is the ship–obstacle distance, ρ_0 is the influence radius of the repulsive force field, and the repulsive force beyond this range is zero.

The repulsive force can be expressed as follows:

$$F_r = \begin{cases} \beta(\frac{1}{\rho} - \frac{1}{\rho_0})\frac{1}{\rho^2}\frac{\partial \rho}{\partial X} & \rho \le \rho_0 \\ 0 & \rho > \rho_0. \end{cases} \tag{27}$$

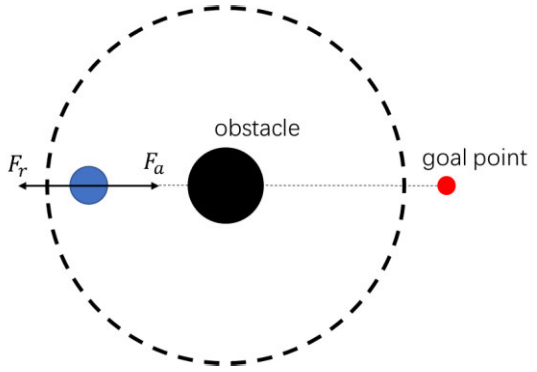

FIGURE 8. Local minimum case in the artificial potential field method.

Finally, through the superposition of repulsion and gravity, the resultant force can be obtained as follows:

$$F = F_a + \sum_{1}^{n} F_r, \tag{28}$$

where n is the total number of obstacles that can affect the ship's force at this time.

B. THE DEFECTS AND IMPROVEMENT OF THE ARTIFICIAL POTENTIAL FIELD METHOD

When the ship, obstacle, and target point are in the same straight line, and the obstacle is in the middle position, the ship will be in a critical state. At this time, the ship's force is balanced, and stagnation or oscillation may occur. In this state, the ship is said to have fallen into the local minimum point (Fig. 8).

When the local minimum is detected, a virtual obstacle is added by evaluating the obstacle distribution to assist the ship in escaping the local minimum point. Virtual obstacles are usually set in a direction perpendicular to the forward direction to provide virtual forces (Fig. 9). By adding virtual obstacles at this time, the resultant force on the ship will be altered, and the virtual obstacles will provide the ship with an additional escape force to evade the local minimum point. In addition, the presence of repulsive force prevents the ship from reentering the minimum point.

The virtual repulsive force field is as follows:

$$U_r' = \begin{cases} \frac{1}{2}\beta'(\frac{1}{\rho'} - \frac{1}{\rho_0'})^2 & \rho' \le \rho_0' \\ 0 & \rho' > \rho_0', \end{cases} \tag{29}$$

where β' is the virtual repulsion potential field constant greater than zero, ρ' is the distance between the ship and the virtual obstacle, ρ_0' is the influence distance of the virtual obstacle on the ship.

Then, the virtual repulsive force is as follows:

$$F_r' = \begin{cases} \beta'(\frac{1}{\rho'} - \frac{1}{\rho_0'})\frac{1}{\rho'^2}\frac{\partial \rho'}{\partial X} & \rho' \le \rho_0' \\ 0 & \rho' > \rho_0'. \end{cases} \tag{30}$$

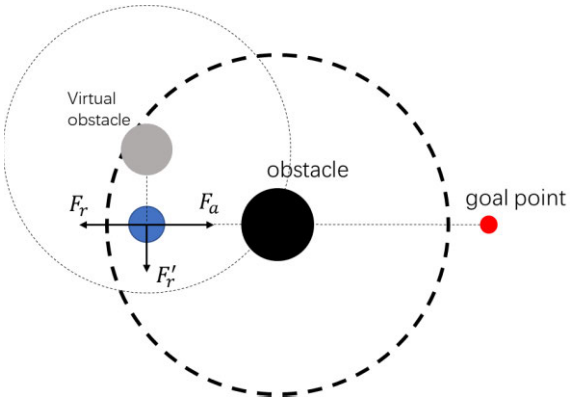

FIGURE 9. Adding virtual obstacle.

The improved repulsive force expression changes the force state by adding virtual obstacles. When determining the position where the ship's force balance enters the local minimum point, introducing virtual obstacles will alter the repulsive force at the position of the point and then change the overall force so that the force is no longer 0, and the local minimum problem can be improved. F_r and F_r' represent the repulsive force of the obstacle and virtual obstacle on the robot, respectively. Combined with the gravity formula of the target point, the resultant force can be expressed as follows:

$$F = F_a + \sum_{1}^{n} F_r + \sum_{1}^{m} F_r'. \tag{31}$$

When the follower tracks the leader's trajectory navigation, if obstacles exist within the follower's perception range, the improved artificial potential field method proposed in this section can be used for local collision avoidance operations. Once the collision danger is removed, the consistency theory is reapplied to track the leader's trajectory and return to the team. Fig. 10 demonstrates the flow chart.

- Step 1: Input the parameters of each ship, such as current position, sailing speed and direction.
- Step 2: Determine whether the ship has entered the influence range of the obstacle, if so, calculate repulsive and gravitational forces, otherwise continue to sail.
- Step 3: When the ship is already affected by the obstacle, whether the resultant force is 0 is judged, if it is 0, add virtual obstacles and then calculate the direction of motion, if not, directly calculate the direction of motion. This step is repeated until it leaves the influence range of the obstacle.
- Step 4: When the ship is out of collision risk, it continues to sail according to the original trajectory.

V. SIMULATION EXPERIMENT

This section focuses on two MATLAB simulations conducted to validate the proposed algorithm's effectiveness. In the first simulation, the USV group path-planning algorithm based on FMS and the leader–follower method is validated in a static environment, whereas the local collision avoidance problem

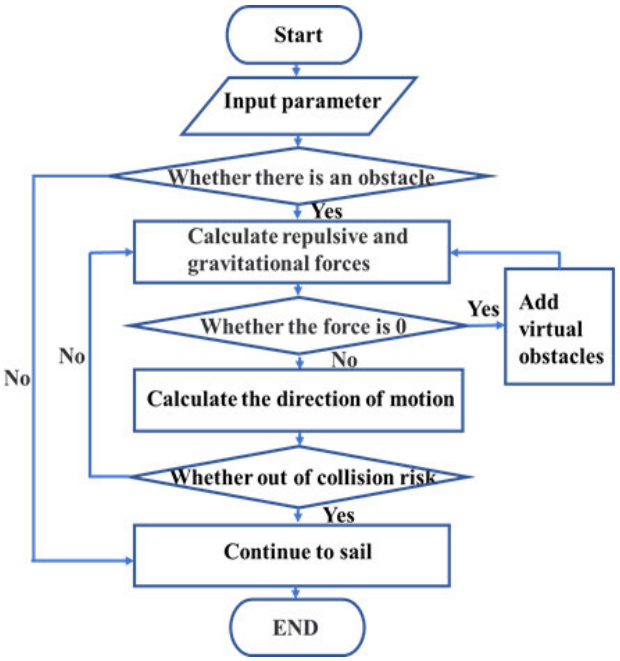

FIGURE 10. Flow chart of improved artificial potential field method.

solved by the improved artificial potential field method is validated in the second simulation.

A. FORMATION PATH PLANNING BASED ON FMS

1) ALGORITHM SIMULATION OF FMM

In this section, we will first verify the path-planning problem based on FMM. Figures are used to demonstrate the steps of the FMM method. In Fig. 11, MATLAB is used to generate an initial map with a size of 200 × 200 pixels, where black areas represent obstacles, such as land or islands, and white areas represent free space. FMM-based USV group path planning is based on this map. Fig. 12 depicts the potential field diagram obtained by first constructing a binary grid diagram, followed by iterating the end point on the figure's propagation surface. Finally, after the above space is established, the gradient descent method is used to iterate continuously from the starting point (marked as a black point in the figure) along the direction of the fastest gradient descent in the generated potential field, and a path with the shortest distance to the end point (marked as a red point in the figure) is obtained (Fig. 13).

Fig. 13 demonstrates that the FMM-obtained path is not smooth and is too close to the obstacle. This is because the essence of FMM is to search for the shortest propagation path of the interface, which prioritizes the length of the path over its safety and smoothness.

2) ALGORITHM SIMULATION OF FMS

The simulation environment uses the same binary grid diagram as FMM. As shown in Fig. 11, cells belonging to obstacles are marked with black, and cells corresponding to the passable area are marked with white. The principle of FMS

FIGURE 11. Initial map.

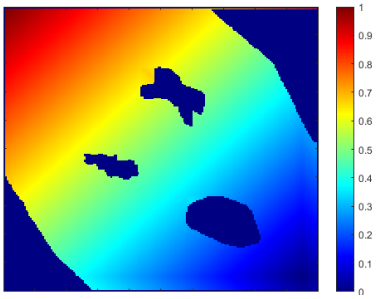

FIGURE 12. Potential field diagram.

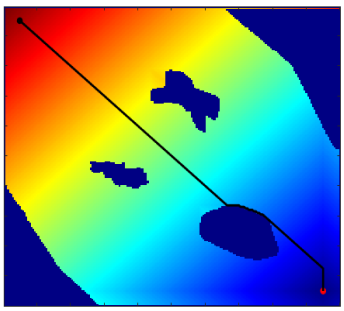

FIGURE 13. Path planning based on FMM.

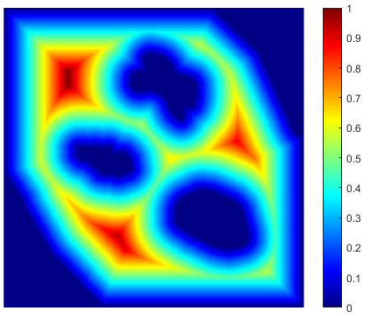

FIGURE 14. Velocity potential field diagram.

route planning is as follows: by applying the initial FMM to iterate over all units regarded as obstacles on the propagation surface of the figure, the velocity potential diagram is obtained, as shown in Fig. 14, where each grid has a value representing its distance from the nearest obstacle, ranging from 0 to 1, and a low value indicates that the current position may be too close to the obstacle, indicating that the USV

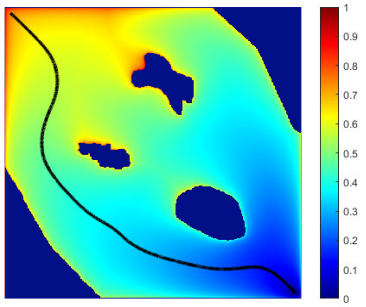

FIGURE 15. Path planning based on FMS.

TABLE 1. Ship's initial information.

	Initial position of ship Unit: km	Initial velocity of the ship Unit: kn	Initial course of the ship
Leader	(0, 0)	15	45°
Follower-1	(−0.2, −0.8)	15	45°
Follower-2	(−1.2, −0.9)	15	45°
Follower-3	(−0.6, 0.5)	15	45°
Follower-4	(−1.4, 1.2)	15	45°

should sail in areas with high values. Subsequently, based on the potential diagram $W(x)$, FMM is reapplied to iterate from the end point on the propagation surface of the diagram, and the potential field diagram is obtained, as shown in the figure. Finally, gradient descent is performed on the entire arrival time map to obtain the optimal path in terms of arrival time, smoothness, and security (Fig. 15).

Notably, the track obtained by path planning using the FMS method is superior in terms of time, security, and smoothness and can be used for the leader's path planning (Fig. 15).

3) FORMATION SIMULATION BASED ON THE LEADER–FOLLOWER METHOD

The first simulation experiment is conducted to verify the stability of the leader–follower method.

The simulation of the USV group path-planning algorithm based on the FMS method includes four followers and a leader. Table 1 lists the initial information of the leader and each follower. As shown in Fig. 16, the leader is represented by a black circle, and the followers are represented by circles of other colors.

The leader sails following the preplanned path, as stipulated in the simulation, to drive in a straight line with uniform speed toward the target point (5, 5). The rest of the followers follow the leader in a preset formation (the two wings are at 60°, and the distance between the two adjacent ships on the same side is 0.2 km). The error distance affects the follower's speed, but to prevent the follower from moving too quickly in the simulation, a maximum speed limit is set for the follower in this experiment.

The trajectory of the ship formation and relative error curves of the leader and each follower are shown in Fig. 17 and Fig. 18. The relative error curve shows that, at about

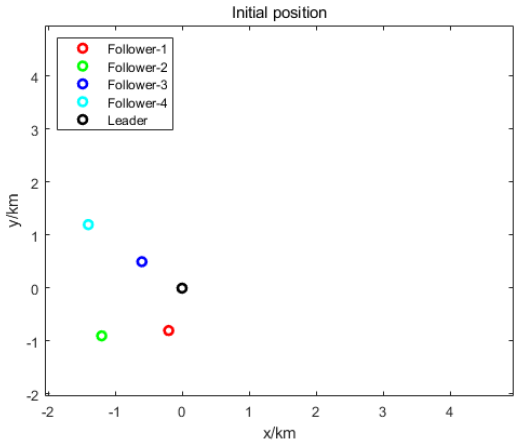

FIGURE 16. Initial position.

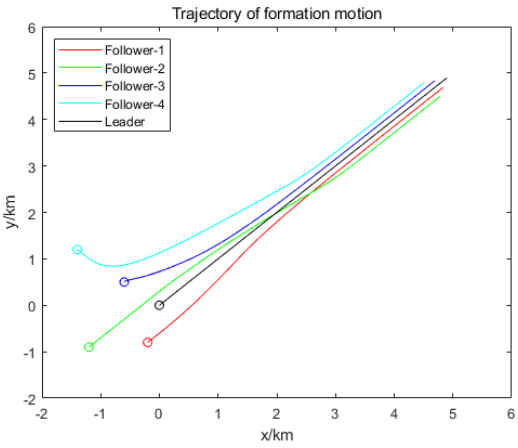

FIGURE 17. Trajectory of formation motion.

FIGURE 18. Position error curve between the leader and each follower.

12 min, all followers reach the preset position and can maintain a stable structure with the leader after that.

Finally, employing the simulation experiment based on FMS in the last section, the leader–follower method is used to define the formation to move forward to the end with the angle between the two wings set at 60°, enabling the follower

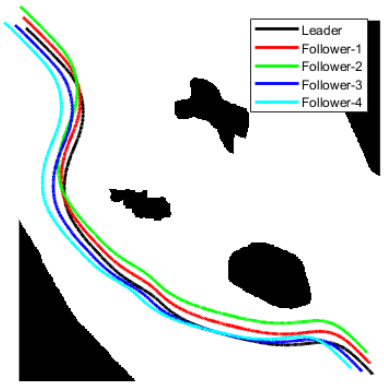

FIGURE 19. Route of a ship formation.

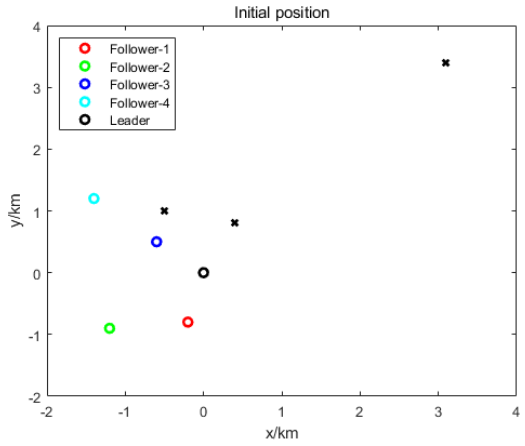

FIGURE 20. Initial position of ship and obstacle.

to maintain the same navigation with the leader. The path curve in this case is shown in Fig. 19. Notably, the method can achieve formation stability and consistency.

B. LOCAL COLLISION AVOIDANCE SIMULATION BASED ON THE IMPROVED ARTIFICIAL POTENTIAL FIELD METHOD

When using the leader–follower method to track the path of the follower to the leader, the collision risk is likely to occur if a situation exists in which the follower is too close to the obstacle on the tracked path. This section simulates the solution to the local collision avoidance problem.

1) ALGORITHM SIMULATION OF THE IMPROVED ARTIFICIAL POTENTIAL FIELD METHOD

The initial information of the leader and each follower is listed in Table 2. As shown in Fig. 20, the leader is represented by a black circle, and followers are represented by circles of other colors.

The preset obstacles are represented by a cross in Fig. 20. The coordinates of the obstacle points are (0.4, 0.8), (−0.5, 1) and (3.1, 3.4). The collision radius of the obstacles is 50 m, and the influence distance is 200 m.

The leader sails following the preplanned path, as stipulated in this experiment, to move toward the target point (5, 5).

TABLE 2. Ship's initial information.

	Initial position of ship Unit: km	Initial velocity of the ship Unit: kn	Initial course of the ship
Leader	(0, 0)	15	45°
Follower-1	(−0.2, −0.8)	15	45°
Follower-2	(−1.2, −0.9)	15	45°
Follower-3	(−0.6, 0.5)	15	45°
Follower-4	(−1.4, 1.2)	15	45°

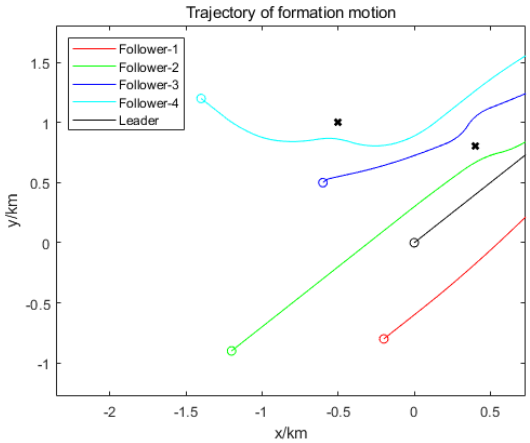

FIGURE 21. Trajectory of formation motion.

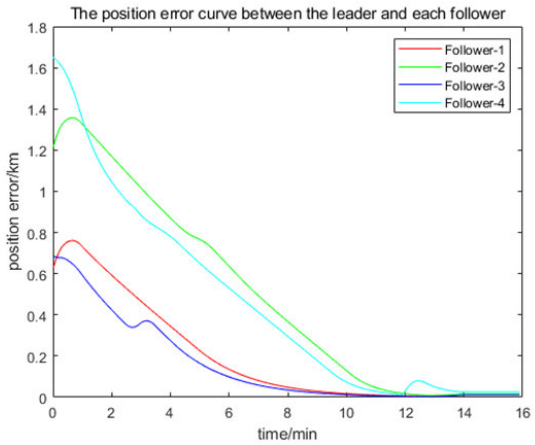

FIGURE 22. The position error curve between the leader and each follower.

The rest of the followers follow the leader in a preset formation (the two wings are at 60°, and the distance between the two adjacent ships on the same side is 0.2 km).

As shown in Fig. 21–24, the follower tracks the leader's path for the first 2 min and 30 s. In 2.7 min, follower-3 senses an obstacle and enters the collision avoidance state. The collision avoidance operation is performed using the improved artificial potential field method, and the collision avoidance is completed in 3.2 min. After the collision avoidance operation is complete, the trajectory points are retracked. The same follower-2 senses an obstacle at 4.6 min and completes the collision avoidance operation at 5.2 min.

Follower-4 appears to be in the same straight line as the obstacle and the path tracking point in the subsequent sailing

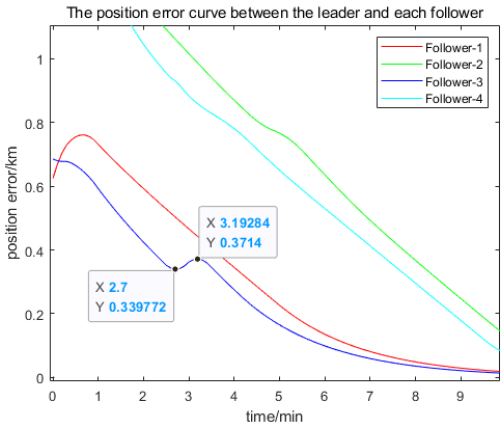

FIGURE 23. Error analysis of follower-3.

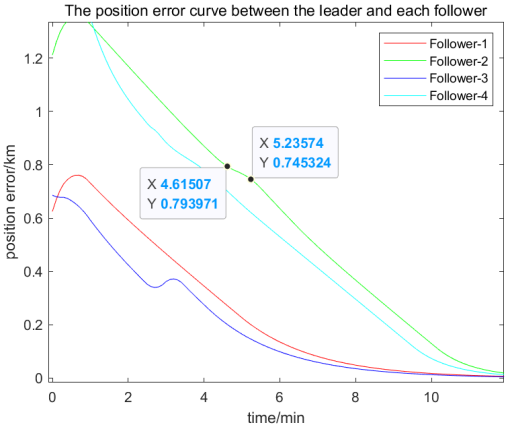

FIGURE 24. Error analysis of follower-2.

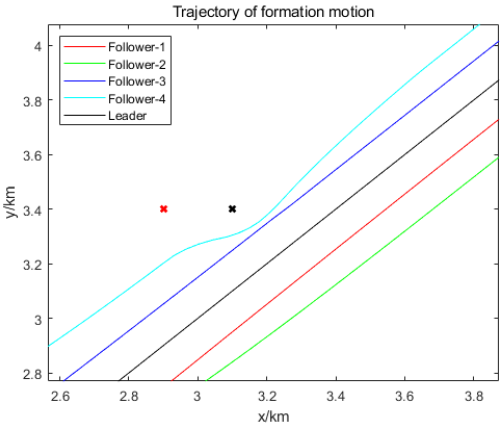

FIGURE 25. Improved artificial potential field method for collision avoidance.

process. At about 12 min, the force balances and falls into the position of the local minimum point. At this time, a virtual obstacle is introduced in the left direction of the object (the red cross in Fig. 25). This virtual obstacle will provide a force perpendicular to the direction of travel, so that the resultant force of the follower is not zero, and the added virtual obstacle prevents the ship from reentering the local minimum point.

Finally, at about 14 min, all followers reach the preset position and maintain a stable structure with the leader after that.

TABLE 3. Ship's initial information.

	Initial position of ship Unit: km	Initial velocity of the ship Unit: kn	Initial course of the ship
Leader	(0.8, 0.8)	15	45°
Follower-1	(0.75, 0.4)	15	45°
Follower-2	(0.6, 0)	15	45°
Follower-3	(0.4, 0.9)	15	45°
Follower-4	(0, 0.6)	15	45°

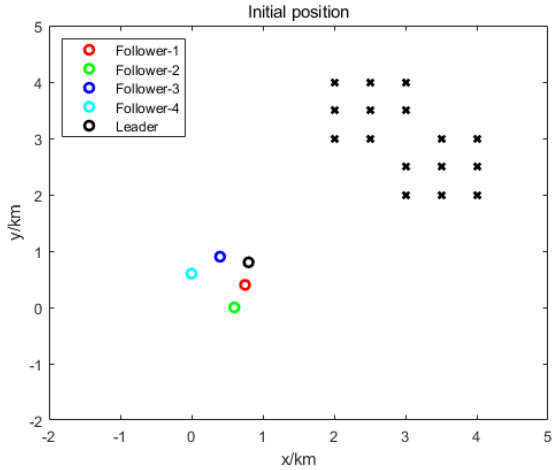

FIGURE 26. Initial position of ship and obstacle.

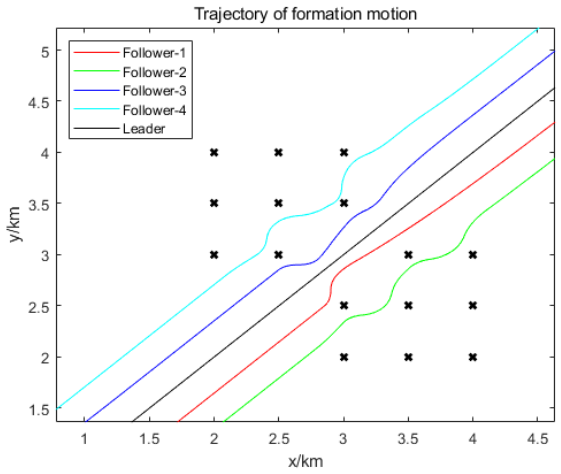

FIGURE 27. Trajectory of formation motion.

2) ALGORITHM SIMULATION OF THE IMPROVED ARTIFICIAL POTENTIAL FIELD METHOD IN MULTI-OBSTACLE ENVIRONMENT

The initial information of the leader and each follower is listed in Table 3. As shown in Fig. 26, the leader is represented by a black circle, and followers are represented by circles of other colors.

The preset obstacles are represented by a cross in Fig. 26.

The leader sails following the preplanned path, as stipulated in this experiment, to move toward the target point (9, 9). The rest of the followers follow the leader in a preset formation (the two wings are at 60°, and the distance between the two adjacent ships on the same side is 0.5 km).

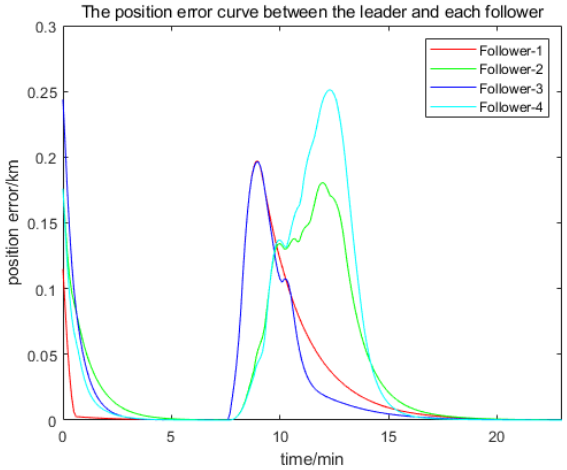

FIGURE 28. The position error curve between the leader and each follower.

As shown in Figures 27-28, the follower enters the multi-obstacle area at about 7.5min and enters the collision avoidance state. Finally regains the stability of the formation at about 17min.

VI. CONCLUSION

The FMS and leader–follower method are combined in this study. The FMS is used to plot a collision-free and smooth course for the ship's sailing reference, after which the consistency theory is used to make the follower track the leader and to realize the effect of formation keeping. In addition, an improved artificial potential field method is proposed to solve the possible obstacles encountered by the follower during navigation, enabling the follower to take collision avoidance behavior independently. This method can effectively prevent the ship from entering the local minimum point position. Meanwhile, after the independent collision avoidance is completed, the consistency theory is reapplied to return the ship to the team. The method and algorithm presented in this paper are verified through computer simulation, and the results demonstrate the method's feasibility.

This study proposes the following ideas for the next stage of research: When the FMS method is used to perform the final step of gradient descent, the selected path is mainly considered to travel in the highest area of the potential field diagram obtained through FMM operation, ensuring the path's safety. However, in some cases, selecting this area is unnecessary, as the navigation's safety may be satisfied in the area above a certain value, suggesting that the selection of a slightly lower area can not only ensure safety but also reduce the distance sailed. Future research will modify the algorithm presented in this study to set a fitness function that balances the speed and safety of the planned path using FMS.

REFERENCES

[1] J. Tang, X. Chen, X. Zhu, and F. Zhu, "Dynamic reallocation model of multiple unmanned aerial vehicle tasks in emergent adjustment scenarios," *IEEE Trans. Aerosp. Electron. Syst.*, early access, Aug. 1, 2022, doi: 10.1109/TAES.2022.3195478.

[2] J. Tang, G. Liu, and Q. Pan, "A review on representative swarm intelligence algorithms for solving optimization problems: Applications and trends," *IEEE/CAA J. Autom. Sinica*, vol. 8, no. 10, pp. 1627–1643, Oct. 2021, doi: 10.1109/JAS.2021.1004129.

[3] C. Pan, Z. Zhang, W. Sun, J. Shi, and H. Wang, "Development of ship weather routing system with higher accuracy using SPSS and an improved genetic algorithm," *J. Mar. Sci. Technol.*, vol. 26, no. 4, pp. 1324–1339, Feb. 2021, doi: 10.1007/s00773-021-00807-z.

[4] P. Zhou, Z. Zhou, Y. Wang, and H. Wang, "Ship weather routing based on hybrid genetic algorithm under complicated sea conditions," *J. Ocean Univ. China*, vol. 22, no. 1, pp. 28–42, Feb. 2023, doi: 10.1007/s11802-023-5002-1.

[5] W. Zhao, Y. Wang, Z. Zhang, and H. Wang, "Multicriteria ship route planning method based on improved particle swarm optimization–genetic algorithm," *J. Mar. Sci. Eng.*, vol. 9, no. 4, p. 357, Mar. 2021, doi: 10.3390/jmse9040357.

[6] W. Zhao, H. Wang, J. Geng, W. Hu, Z. Zhang, and G. Zhang, "Multi-objective weather routing algorithm for ships based on hybrid particle swarm optimization," *J. Ocean Univ. China*, vol. 21, no. 1, pp. 28–38, Feb. 2022, doi: 10.1007/s11802-022-4709-8.

[7] J. Li, H. Wang, W. Zhao, and Y. Xue, "Ship's trajectory planning based on improved multiobjective algorithm for collision avoidance," *J. Adv. Transp.*, vol. 2019, pp. 1–12, Apr. 2019, doi: 10.1155/2019/4068783.

[8] J. Li, H. Wang, Z. Guan, and C. Pan, "Distributed multi-objective algorithm for preventing multi-ship collisions at sea," *J. Navigat.*, vol. 73, no. 5, pp. 971–990, Sep. 2020, doi: 10.1017/S0373463320000053.

[9] G. Zhang, Y. Wang, J. Liu, W. Cai, and H. Wang, "Collision-avoidance decision system for inland ships based on velocity obstacle algorithms," *J. Mar. Sci. Eng.*, vol. 10, no. 6, p. 814, Jun. 2022, doi: 10.3390/jmse10060814.

[10] Y. Wang, Y. Zhang, H. Zhao, and H. Wang, "Assessment method based on AIS data combining the velocity obstacle method and Pareto selection for the collision risk of inland ships," *J. Mar. Sci. Eng.*, vol. 10, no. 11, p. 1723, Nov. 2022, doi: 10.3390/jmse10111723.

[11] M. Saad, A. I. Salameh, S. Abdallah, A. El-Moursy, and C.-T. Cheng, "A composite metric routing approach for energy-efficient shortest path planning on natural terrains," *Appl. Sci.*, vol. 11, no. 15, p. 6939, Jul. 2021, doi: 10.3390/app11156939.

[12] W. Zhang, D. Xia, G. Chang, Y. Hu, Y. Huo, F. Feng, Y. Li, and H. Li, "APFD: An effective approach to taxi route recommendation with mobile trajectory big data," *Frontiers Inf. Technol. Electron. Eng.*, vol. 23, no. 10, pp. 1494–1510, Sep. 2022, doi: 10.1631/FITEE.2100530.

[13] H. Niu, Z. Ji, A. Savvaris, and A. Tsourdos, "Energy efficient path planning for unmanned surface vehicle in spatially-temporally variant environment," *Ocean Eng.*, vol. 196, Jan. 2020, Art. no. 106766, doi: 10.1016/j.oceaneng.2019.106766.

[14] X. Chen, N. Bose, M. Brito, F. Khan, G. Millar, C. Bulger, and T. Zou, "Risk-based path planning for autonomous underwater vehicles in an oil spill environment," *Ocean Eng.*, vol. 266, Dec. 2022, Art. no. 113077, doi: 10.1016/j.oceaneng.2022.113077.

[15] X. Tong, S. Yu, G. Liu, X. Niu, C. Xia, J. Chen, Z. Yang, and Y. Sun, "A hybrid formation path planning based on A* and multi-target improved artificial potential field algorithm in the 2D random environments," *Adv. Eng. Informat.*, vol. 54, Oct. 2022, Art. no. 101755, doi: 10.1016/j.aei.2022.101755.

[16] L. Wang, Z. Zhang, Q. Zhu, and S. Ma, "Ship route planning based on double-cycling genetic algorithm considering ship maneuverability constraint," *IEEE Access*, vol. 8, pp. 190746–190759, 2020, doi: 10.1109/ACCESS.2020.3031739.

[17] W. Lu and M. Wu, "Optimization of vehicle automatic navigation path based on remote sensing and GIS," *Optik*, vol. 270, Nov. 2022, Art. no. 169952, doi: 10.1016/j.ijleo.2022.169952.

[18] H.-B. Wang, X.-G. Li, P.-F. Li, E. I. Veremey, and M. V. Sotnikova, "Application of real-coded genetic algorithm in ship weather routing," *J. Navigat.*, vol. 71, no. 4, pp. 989–1010, Jul. 2018, doi: 10.1017/S0373463318000048.

[19] E. Krell, S. A. King, and L. R. Garcia Carrillo, "Autonomous surface vehicle energy-efficient and reward-based path planning using particle swarm optimization and visibility graphs," *Appl. Ocean Res.*, vol. 122, May 2022, Art. no. 103125, doi: 10.1016/j.apor.2022.103125.

[20] J. Zhong, B. Li, S. Li, F. Yang, P. Li, and Y. Cui, "Particle swarm optimization with orientation angle-based grouping for practical unmanned surface vehicle path planning," *Appl. Ocean Res.*, vol. 111, Jun. 2021, Art. no. 102658, doi: 10.1016/j.apor.2021.102658.

[21] A. Serani, G. Fasano, G. Liuzzi, S. Lucidi, U. Iemma, E. F. Campana, F. Stern, and M. Diez, "Ship hydrodynamic optimization by local hybridization of deterministic derivative-free global algorithms," *Appl. Ocean Res.*, vol. 59, pp. 115–128, Sep. 2016, doi: 10.1016/j.apor.2016.04.006.
[22] G. Zhang, H. Wang, W. Zhao, Z. Guan, and P. Li, "Application of improved multi-objective ant colony optimization algorithm in ship weather routing," *J. Ocean Univ. China*, vol. 20, no. 1, pp. 45–55, Jan. 2021, doi: 10.1007/s11802-021-4436-6.
[23] E. W. Dijkstra, "A note on two problems in connexion with graphs," *Numer. Math.*, vol. 1, no. 1, pp. 269–271, Dec. 1959, doi: 10.1007/BF01386390.
[24] P. E. Hart, N. J. Nilsson, and B. Raphael, "Correction to a formal basis for the heuristic determination of minimum cost paths," *ACM SIGART Bull.*, no. 37, pp. 28–29, Dec. 1972, doi: 10.1145/1056777.1056779.
[25] A. S. James, *Level Set Methods and Fast Marching Methods*. New York, NY, USA: Cambridge Univ. Press, 1996.
[26] Z. Guan, Y. Wang, Z. Zhou, and H. Wang, "Research on early warning of ship danger based on composition fuzzy inference," *J. Mar. Sci. Eng.*, vol. 8, no. 12, p. 1002, Dec. 2020, doi: 10.3390/jmse8121002.
[27] M. Shang, M. Chu, and M. Grethler, "Path planning based on artificial potential field and fuzzy control," in *Proc. IEEE Int. Conf. Power Electron., Comput. Appl.*, Mar. 2021, pp. 304–308, doi: 10.1109/ICPECA51329.2021.9362519.
[28] X. Yang, "Development of obstacle avoidance for autonomous vehicles and an optimization scheme for the artificial potential field method," in *Proc. 2nd Int. Conf. Comput. Data Sci. (CDS)*, Jan. 2021, pp. 12–18, doi: 10.1109/CDS52072.2021.00010.
[29] Z. Xin, X. Rongwu, and C. Guo, "AUV path planning in dynamic environment based on improved artificial potential field method based on visibility graph," *J. Phys., Conf.*, vol. 2383, no. 1, Dec. 2022, Art. no. 012090, doi: 10.1088/1742-6596/2383/1/012090.
[30] L. Liu, B. Wang, and H. Xu, "Research on path-planning algorithm integrating optimization A-star algorithm and artificial potential field method," *Electronics*, vol. 11, no. 22, p. 3660, Nov. 2022, doi: 10.3390/electronics11223660.
[31] C. Zheyi and X. Bing, "AGV path planning based on improved artificial potential field method," in *Proc. IEEE Int. Conf. Power Electron., Comput. Appl. (ICPECA)*, Jan. 2021, pp. 32–37, doi: 10.1109/ICPECA51329.2021.9362519.
[32] J. Wang, R. Wang, D. Lu, H. Zhou, and T. Tao, "USV dynamic accurate obstacle avoidance based on improved velocity obstacle method," *Electronics*, vol. 11, no. 17, p. 2720, Aug. 2022, doi: 10.3390/electronics11172720.
[33] T. Xu, S. Zhang, Z. Jiang, and Z. Liu, "Collision avoidance of high-speed obstacles for mobile robots via maximum-speed aware velocity obstacle method," *IEEE Access*, vol. 8, pp. 138493–138507, 2020, doi: 10.1109/ACCESS.2020.3012513.
[34] R. Skjetne, S. Moi, and T. I. Fossen, "Nonlinear formation control of marine craft," in *Proc. 41st IEEE Conf. Decis. Control.*, Dec. 2002, pp. 1699–1704, doi: 10.1109/CDC.2002.1184765.
[35] I.-A.-F. Ihle, M. Arcak, and T. I. Fossen, "Passivity-based designs for synchronized path-following," *Automatica*, vol. 43, no. 9, pp. 1508–1518, Sep. 2007, doi: 10.1016/j.automatica.2007.02.018.
[36] R. Ghabcheloo, A. P. Aguiar, A. Pascoal, C. Silvestre, I. Kaminer, and J. Hespanha, "Coordinated path-following control of multiple underactuated autonomous vehicles in the presence of communication failures," in *Proc. 45th IEEE Conf. Decis. Control*, Dec. 2006, pp. 4345–4350, doi: 10.1109/CDC.2006.376989.
[37] M. Breivik, V. E. Hovstein, and T. I. Fossen, "Straight-line target tracking for unmanned surface vehicles," *Model., Identificat. Control, Norwegian Res. Bull.*, vol. 29, no. 4, pp. 131–149, 2008, doi: 10.4173/MIC.2008.4.2.
[38] R. Cui, S. Sam Ge, B. Voon Ee How, and Y. Sang Choo, "Leader–follower formation control of underactuated autonomous underwater vehicles," *Ocean Eng.*, vol. 37, nos. 17–18, pp. 1491–1502, Dec. 2010, doi: 10.1016/j.oceaneng.2010.07.006.
[39] I.-A.-F. Ihle, J. Jouffroy, and T. I. Fossen, "Formation control of marine surface craft: A Lagrangian approach," *IEEE J. Ocean. Eng.*, vol. 31, no. 4, pp. 922–934, Oct. 2006, doi: 10.1109/JOE.2006.880426.
[40] F. Huang, P. Wu, and X. Li, "Distributed flocking control of quad-rotor UAVs with obstacle avoidance under the parallel-triggered scheme," *Int. J. Control, Autom. Syst.*, vol. 19, no. 3, pp. 1375–1383, Jan. 2021, doi: 10.1007/s12555-019-0315-y.
[41] G. Sun, R. Zhou, B. Di, and H. Yu, "A physicochemically inspired approach to flocking control of multiagent system," *Nonlinear Dyn.*, vol. 102, pp. 2627–2648, Nov. 2020, doi: 10.1007/s11071-020-06062-y.
[42] M. Fernando, "Online flocking control of UAVs with mean-field approximation," in *Proc. IEEE Int. Conf. Robot. Autom. (ICRA)*, May 2021, pp. 8977–8983, doi: 10.1109/ICRA48506.2021.9560899.
[43] L. Ding and G. Guo, "Formation control for ship fleet based on backstepping," *Control Decis.*, vol. 27, no. 2, pp. 299–303, 2012.
[44] B. Liu, T. Chu, L. Wang, and G. Xie, "Controllability of a leader–follower dynamic network with switching topology," *IEEE Trans. Autom. Control*, vol. 53, no. 4, pp. 1009–1013, May 2008, doi: 10.1109/TAC.2008.919548.
[45] S. A. Ajwad, T. Ménard, E. Moulay, M. Defoort, and P. Coirault, "Observer based leader-following consensus of second-order multi-agent systems with nonuniform sampled position data," *J. Franklin Inst.*, vol. 356, no. 16, pp. 10031–10057, Nov. 2019, doi: 10.1016/j.jfranklin.2019.09.025.
[46] Q. Wang, K. Liu, X. Wang, L. Wu, and J. Lv, "Leader-following consensus of multi-agent systems under antagonistic networks," *Neurocomputing*, vol. 413, pp. 339–347, Nov. 2020, doi: 10.1016/j.neucom.2020.07.006.
[47] O. Khatib, "Real-time obstacle avoidance for manipulators and mobile robots," *Int. J. Robot. Res.*, vol. 5, no. 1, pp. 90–98, Mar. 1986, doi: 10.1177/027836498600500106.

MINGYANG LI was born in Siping, China, in 1998. He received the bachelor's degree in electronic information science and technology from Jilin University, Jilin, in 2020, where he is currently pursuing the M.D. degree in circuits and systems. His research interest includes ship formation algorithm.

KAI MENG was born in Xuzhou, China, in 1998. He received the bachelor's degree in electronic and information engineering from Yangzhou University, Jiangsu, in 2021. He is currently pursuing the M.D. degree in circuits and systems with Jilin University. His research interests include localization and navigation.

JIELU CHEN was born in Nantong, China, in 1988. She received the master's degree in computer science and engineering from Shanghai Jiao Tong University, in 2020. Her research interest includes navigation automation based on auto-pilot.

HONGBO WANG (Member, IEEE) was born in Changchun, China, in 1969. She received the Ph.D. degree from Saint Petersburg State University, Russia. She is currently with the College of Electronic Science and Engineering, Jilin University. Her research interests include ship motion control, weather routing, and ship collision avoidance.